Strongly nonparabolic variation of the band gap in $In_xAl_{1-x}N$ with low indium content

Vitaly Z. Zubialevich[1,a)], Duc V. Dinh[1], Shahab N. Alam[1,2], Stefan Schulz[1], Eoin P. O'Reilly[1,3] and Peter J. Parbrook[1,2]

[1] Tyndall National Institute, University College Cork, Lee Maltings, Dyke Parade, Cork, Ireland

[2] School of Engineering, University College Cork, Cork, Ireland

[3] Department of Physics, University College Cork, Cork, Ireland

80-120 nm thick $In_xAl_{1-x}N$ epitaxial layers with $0 < x < 0.224$ were grown by metalorganic vapour phase epitaxy on AlN/Al_2O_3-templates. The composition was varied through control of the growth temperature. The composition dependence of the band-gap was estimated from the photoluminescence excitation absorption edge for $0 < x < 0.11$ as the material with higher In content showed no luminescence under low excitation. A very rapid decrease in band-gap was observed in this range, dropping down below 5.2 eV at $x = 0.05$, confirming previous theoretical work that used a band-anticrossing model to describe the strongly x-dependent bowing parameter, which in this case exceeds 25 eV in the $x \rightarrow 0$ limit. A double absorption edge observed for InAlN with $x < 0.01$ was attributed to crystal-field splitting of the highest valence band states. Our results indicate also that the ordering of the valence bands is changed at much lower In contents than one would expect from linear interpolation of the valence band parameters. These findings on band-gap bowing and valence band ordering are of direct relevance for the design of InAlN-containing optoelectronic devices.

Keywords: InAlN, band-gap, band-gap bowing parameter, photoluminescence excitation.

[a)] E-mail: vitaly.zubialevich@tyndall.ie

1. Introduction

In the last several years InAlN ternary alloys have found practical application mostly in Bragg reflectors [1] and high electron mobility transistors [2] due to the possibility of lattice matching to GaN. In addition, polarisation matching to AlGaN can be achieved with InAlN, allowing an increased freedom in heterostructure engineering for various other applications [3, 4]. Recently the potential was demonstrated to use InAlN as the active region of light emitting heterostructures in the near UV spectral range [5]. To design InAlN-based optoelectronic devices operating in the UV spectral range, a knowledge of the variation of the band gap with alloy composition is of central importance, especially in the low In content regime. In addition to its use in a device active region, it also has potential for AlInN/Al(Ga)N Bragg reflectors in the solar blind spectral region for detector applications. [6]. Despite the interest in InAlN alloys the band-gap variation with composition has not yet been determined unambiguously across the entire composition range, with a fairly large spread in the reported experimental values even for the most studied and technologically important composition range close to lattice match to GaN [7, 8]. In addition to the predicted composition immiscibility [9], a further uncertainty relates to the recently reported role of Ga autoincorporation [10, 11] which, depending on reactor design, can occur in InAlN grown by metalorganic vapour phase epitaxy if no special efforts are undertaken to suppress it. In spite of the scatter of experimental data it is clear that the virtual crystal approximation [12] fails for $In_xAl_{1-x}N$ which, unlike AlGaN or InGaN, cannot be described with a single composition-independent band-gap bowing parameter. It was shown both experimentally [7, 13] and theoretically [8, 14, 15] that the bowing parameter is instead essentially composition-dependent, varying from around 3 eV for high indium contents ($x > 0.8$) to presumably more than 10 eV for $x < 0.1$.

In addition to the band gap variation, the light polarization characteristic of InAlN-based devices are important, since light extraction efficiencies of the device are significantly affected by this property [16]. The light polarization characteristic is related to the valence band ordering in the InAlN material; in Al-rich InAlN systems, a transverse magnetic (TM) optical emission is expected.

In this case the emitted light is polarised along the wurtzite c-axis. With increasing In content, due to changes in the valence band structure, the emission switches to be transverse electric (TE). For surface emitting light emitting diodes, TE polarization is vital for high light extraction efficiency, and therefore for device design the information on this crossover is important. Recently, it has been shown theoretically [8] that in InAlN it might appear at much lower In contents than one would expect from a linear interpolation of the valence band parameters. However, to analyse this experimentally, low In content InAlN has to be studied.

In this paper we use photoluminescence excitation (PLE) spectroscopy to present a detailed study of the room temperature $In_xAl_{1-x}N$ band-gap for the $0 < x < 0.11$ range. There is only a little data in the literature on the band-gap of low indium content InAlN [17], due to the focus of attention in this material system being on compositions close to the lattice-matching condition with GaN ($x = 0.17$). Hence the majority of discussion on the variation and strength of the bowing parameter for $x < 0.1$ has been based on extrapolation of the InAlN band-gap dependence in the range $0.1 < x < 0.25$ to the low x region. This extrapolation has been based on the rather scattered array of published data available for such indium contents [7], or else on theoretical calculations [8, 18], which still need to be supported by experiment. Good quality InAlN in this range should be grown on thick (few μm) AlN templates. This causes difficulties in estimation of the band-gap by most of the available techniques particularly for low x, in addition to the general complications of working in the deep ultraviolet spectral range. Absorption/transmittance measurements are hampered due to a strong contribution from the sub band-gap absorption tail of the much thicker AlN layer. Any ellipsometry measurement of the InAlN/AlN heterostructure is also mostly defined by the thicker AlN layer and its analysis becomes complicated/less reliable for low indium content InAlN. Reflectance spectra will also be dominated by AlN excitonic features. Band-gap estimation from the onset of interference fringes in reflectance spectra can be carried out only for relatively thick InAlN layers, which are difficult to controllably prepare.

Our report of the $In_xAl_{1-x}N$ band-gap for $x < 0.11$ is free of the disadvantages of the above mentioned methods, because no room temperature PL is detected from the AlN templates under the weak excitation conditions used, while fairly strong PL was observed from the InAlN epilayers. This makes our PLE measurement insensitive to the presence of the thick AlN template, and allows precise analysis of the InAlN absorption edge. We first present the procedures used to prepare the material and then to determine the InAlN composition and band-gap. Particular attention is paid to the presence of valence band intermixing and the effect this has on the PLE spectra. Finally a discussion is presented of the nature of the change in band-gap with increasing In composition. We show that the observed behaviour can be well described and understood using a band-anticrossing (BAC) model to treat the interaction of In-related localised states with the alloy conduction and valence band edges.

2. Experimental

All samples studied here were grown by metalorganic vapour phase epitaxy (MOVPE) in a 3x2" AIXTRON showerhead reactor using trimethylindium (TMIn), trimethylaluminium (TMAl) and ammonia as precursors. The 80-100 nm thick $In_xA_{1-x}lN$ epilayers were grown on 2.5 μm AlN-templates on *c*-Al_20_3 prepared under conditions as reported elsewhere [19]. The In composition, *x,* was varied from below 0.01 to 0.224 using growth temperatures T_g in the range 940°C to 730°C. A high V/III ratio of 3600, TMIn/TMAl ratio of 0.5, pressure of 70 mbar and nitrogen ambient were used for InAlN; the growth rate at such conditions was about 0.05 nm/s, decreasing slightly with increasing temperature.

As mentioned above, MOVPE grown InAlN often suffers from Ga autoincorporation. We undertook a number of measures to almost completely eliminate this unwanted process in our samples. Firstly the showerhead was thoroughly cleaned, reactor glassware changed, and the susceptor baked at high temperature prior to growth of the sample series. This was followed by the growth of a number of AlN-templates to coat the reactor chamber. No deposition using trimethylgallium was undertaken until the last sample in this reported series had been grown. This

reduced the Ga content in our samples down to negligible levels, as confirmed by secondary ion mass spectrometry measurements for the $In_{0.045}Al_{0.955}N$ sample, where a value of less than 0.001 (0.1%) was estimated. Taking into account the AlGaN band-gap bowing parameter of 1 eV [20], this would lead to no more than 4 meV of additional narrowing of the band-gap in comparison to the case of an absolutely Ga-free InAlN layer.

All samples were characterized by X-ray diffraction (XRD) using a PANalytical X'pert PRO XRD system. Symmetric 0002 ω-2Θ scans and asymmetric 10-15 reciprocal space maps were carried out to determine the indium content and strain status of the samples.

Photoluminescence (PL) was excited using a double monochromator coupled Xe-lamp at room temperature (RT, 295 K). PL and PLE spectra were detected using an iHR320 Horiba imaging spectrometer equipped with a photomultiplier. PL spectra were excited with the wavelengths corresponding to the maxima of their PLE spectra and divided by the intensity of the Xe-lamp at the same wavelengths. To replot the PL spectra versus photon energy, the measured spectra were divided by the square of the photon energy:

$$I_{\mathrm{PL}}(h\nu) = \frac{I_{\mathrm{PL}}(\lambda)}{h\nu^2}. \tag{1}$$

Relative PL efficiencies of the samples were calculated as integrals of their PL spectra plotted using Eq. (1) divided by intensities of the Xe-lamp emission at wavelengths used for their excitation. The PL spectrum position $h\nu_{\mathrm{PL}}$ used here was defined as the centre-weighted PL spectrum position given by the expression:

$$h\nu_{\mathrm{PL}} = \frac{\int_{h\nu_{\mathrm{min}}}^{h\nu_{\mathrm{max}}} \xi \cdot I_{\mathrm{PL}}(\xi) d\xi}{\int_{h\nu_{\mathrm{min}}}^{h\nu_{\mathrm{max}}} I_{\mathrm{PL}}(\xi) d\xi}, \tag{2}$$

where ($h\nu_{\mathrm{min}}$, $h\nu_{\mathrm{max}}$) is the photon energy range, within which $I_{\mathrm{PL}} > 0$, and ξ is an integration variable. The PLE spectra were fitted with a sigmoidal function [21] to derive the effective band-gap $E_{\mathrm{g,\,eff}}$ of

the samples studied. A double sigmoidal function was used to analyse the PLE spectra of those samples which exhibited a double absorption edge in PLE.

3. Results and discussion

The change in composition of the $In_xAl_{1-x}N$ layers determined by XRD with growth temperature is presented by the square and circle datapoints in Fig. 1; the PL data (diamonds and triangles) will be discussed later. In the temperature range $T_g > 800$°C, x was found to decrease exponentially with T_g. The growth rates for nitrides of each III group metal are proportional to the difference between the rates of metal adsorption onto the growth surface and desorption from it. One can neglect the temperature dependence of the growth rate for AlN, since the Al adatom sticking coefficient is considered to be unity in the studied temperature range [22]. However, the InN growth rate should drop with T_g much faster than exponentially. The indium adsorption rate does not depend strongly on T_g, but its desorption rate increases rapidly with T_g. Thus, the InN growth rate should also rapidly decrease with growth temperature, reaching even negative values when the In desorption rate exceeds that of its adsorption. This would lead to a similar rapid decrease of x with T_g in our samples. The relatively slow exponential decrease of x observed in our experiment may be due to a decreased desorption rate of In ad-atoms once they are surrounded by Al ones. The indium content x is therefore driven by the probability of an In adatom being surrounded by Al adatoms before desorption can occur, rather than being determined by the pure In adatom desorption rate. It is reasonable that even at fairly high T_g a small amount of In adatoms has a chance to be surrounded by Al adatoms before their desorption.

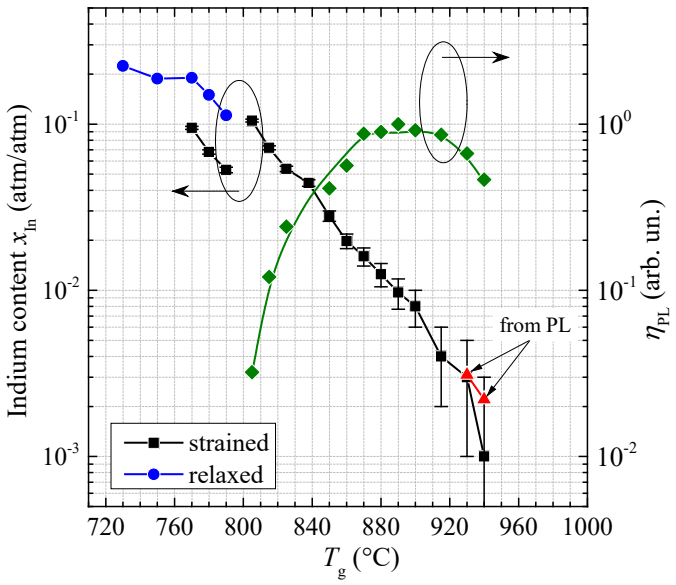

Fig. 1. Dependence of InAlN indium content on growth temperature as determined from XRD (squares and circles) and PL measurements (triangles). For an explanation of the data from PL, see text below. Growth temperature dependent PL efficiency is shown by diamonds.

It was found from analysis of symmetric 0002 ω-2Θ and asymmetric 10-15 reciprocal space map XRD measurements that $In_xAl_{1-x}N$ layers of ~100 nm thickness are fully strained if $T_g > 825$°C, corresponding to $x < 0.054$, with samples in the range ($805°C \leq T_g \leq 825°C$; $0.105 \geq x \geq 0.054$) showing only slight relaxation (about 25% for the $x = 0.105$ sample). A strong RT PL band was observed for these strained InAlN layers, centred between 310 and 370 nm and with full width at half maxima (FWHM) within the 0.66-0.97 eV range, as shown in Fig. 2. At growth temperatures lower than 805°C, the material splits into two subsystems with different stress status and composition (Fig. 1, squares and circles). No luminescence was observed from the samples with $x > 0.11$, which is attributed to the high defect density in these mismatched and relaxed layers implied by the XRD data. This appears in a strong broadening of 0002 and especially 1-101 ω-scans of this relaxed layers relative to those for AlN-templates used (250-350" and 550-650" for 0002 and 1-101 reflectances, respectively), while the strained layers are characterised by FWHMs within only 10% difference from them. It is worth noting that the relative RT PL efficiency of the UV band, having a maximum at around $x = 0.01$ (Fig. 1, diamonds), starts to drop significantly even before x reaches the value beyond which relaxation is clearly detected by XRD. This may indicate that the decrease in PL efficiency is

not only due to an initial relatively weak relaxation not yet clearly seen in XRD, but also due to a possible increase of point defect concentration at lower growth temperatures [23].

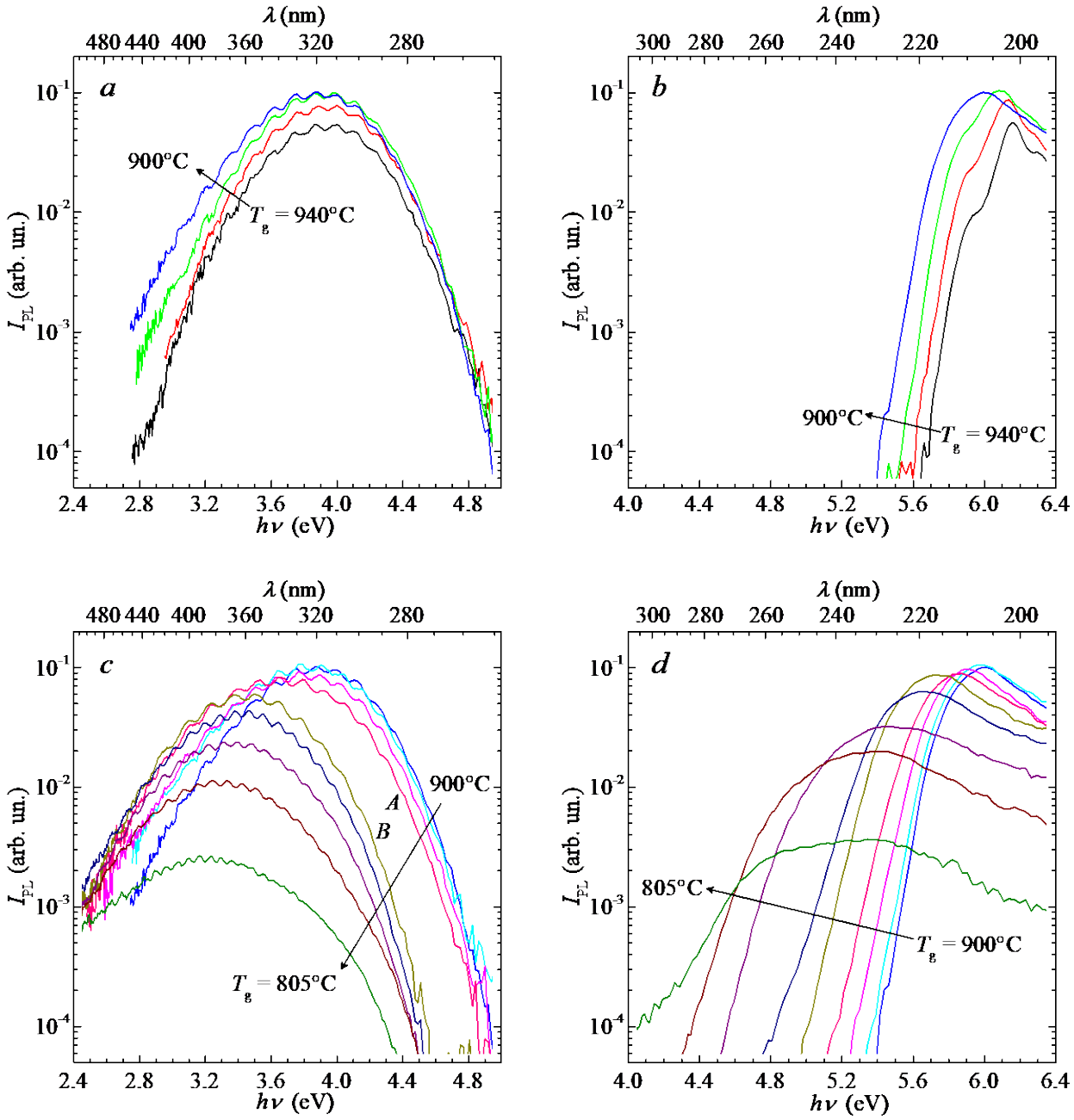

Fig. 2. RT PL (*a*, *c*) and PLE (*b*, *d*) spectra of InAlN layers grown at different temperatures.

Chichibu et al. [24] recently observed a similar near-UV band in *m*-plane $In_{0.02}Al_{0.98}N$ samples, which they proposed to be possibly due to carbon or Al vacancies. To investigate if this is the origin of the PL in our case, we analysed AlN layers grown firstly under optimised conditions for our AlN template (see Ref. [19] for growth details), and secondly under the conditions used to prepare the

InAlN samples (only eliminating the TMIn flow rate, i.e. $x = 0$). In both cases, the AlN samples were found to be optically inactive (no PL signal detected) under the weak excitation conditions used (~10^{-5} W/cm^2 power density at 198 nm emission wavelength from the spectrometer coupled Xe-lamp). At the same time, the samples become immediately luminescing if even a small fraction of Al atoms is substituted by In atoms as shown in Fig. 2. We thus consider a luminescence centre involving In, possibly in complex with carbon or with Al vacancies, as the origin of the luminescence, rather than carbon or Al vacancies on their own. Taking into account the very large PL Stokes shift of about 1.9 eV in these low x samples, it is difficult to interpret the observed PL band as a band-edge emission; the exact nature of this band is currently unknown and is beyond the scope of the present work.

Fig. 3 shows that the InAlN PL spectrum blue-shifts with increasing T_g until 915°C, but then saturates as the temperature is further increased, as can also be seen in Fig. 2, *a* and *c*. The PL band FWHM decreases from 0.81 eV at T_g = 870°C to 0.66 eV at T_g = 915°C, with this decrease saturating for higher T_g. Thus, the PL spectrum shape and position becomes in essence independent of growth temperature and therefore of indium content for $T_g \geq 915$°C ($x \leq 0.004$). At the same time the PL efficiency, having been nearly stable across the 870°C < T_g < 915°C range, starts to drop distinctly with further increasing T_g. The absence of the UV PL band for the AlN samples, combined with its presence in the InAlN samples, and the correlation of its efficiency with indium content at small x support our argument that In-related centres are involved in the luminescence mechanism. Moreover, it is reasonable to assume that the PL efficiency of the InAlN samples grown at the highest temperatures (≥ 915°C) is proportional to the indium content in them, therefore allowing a second method to estimate composition. Using the $In_{0.004}Al_{0.996}N$ sample as a reference and assuming a linear dependence of the PL efficiency with indium content, the x values of the two highest growth temperature samples were estimated using the simple expression:

$$x = x_0 \frac{\eta_{\mathrm{PL},\,x}}{\eta_{\mathrm{PL},\,x_0}}, \tag{3}$$

where x_0 and $\eta_{\mathrm{PL},\,x_0}$ are 0.004 and the PL efficiency of the $In_{0.004}Al_{0.996}N$ sample, respectively, and $\eta_{\mathrm{PL},\,x}$ is the PL efficiency of the sample for which the x value is being estimated. These indium composition estimates are included in Fig. 1 (triangular data points marked as "from PL"). It is clear that a key challenge in examining such low composition alloys is the determination of the composition at such small values, leading to the increasing error bars shown in Fig. 1. Using the monotonic decrease in efficiency as a predictor, the additional estimate of x can be made for the samples grown at highest T_g, where the error in estimation of x from XRD is ±0.002 and thus exceeds 50% of the absolute value of x. It is worth noting that the "from PL" x value for the sample grown at 930°C and its XRD estimate are very close, while the PL based estimate for the sample grown at the highest T_g is still within the error bar of the XRD measurement. The "from PL" values also lie close to what might be predicted based on extrapolation of composition with temperature for the series as a whole, based on the data in Fig. 1. We therefore use these "from PL" x values for the samples grown at the two highest T_g as our best estimate of the composition.

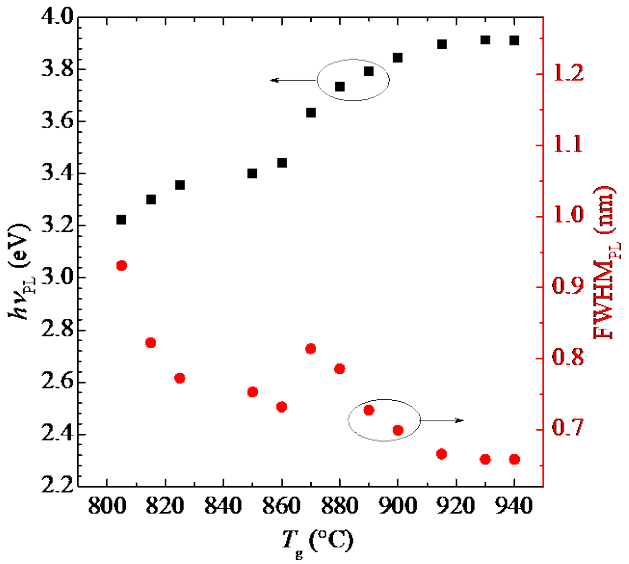

Fig. 3. PL spectrum position (squares) and FWHM (circles) of InAlN layers as a function of growth temperature.

There is a significant jump in the evolution of the PL spectra with T_g between 860°C and 870°C (as plotted in Fig. 2, *c*, curves *A* and *B*, respectively) with a change in peak position and, more

dramatically, FWHM being observed (Fig. 3). The samples were grown sequentially, with no substantial change in growth conditions identified other than the change in growth temperature. The reason for the sudden change in behaviour is unclear, though it is likely, given the behaviour of the PL FWHM in particular, that the band is made of two different sources: for example deep centres involving single In atoms for higher T_g and those involving multiple ones for lower T_g, with competition between them leading to the single In atom-related one collapsing at lower T_g due to a higher occurrence of clusters of multiple In atoms and carrier localisation in them. To support this conjecture it is worth noting that for low x, $In_xAl_{1-x}N$ can be considered as an ensemble of separate In atoms in the AlN matrix and therefore the PL spectra observed for $x \leq 0.004$ are associated with the presence of such atoms. This would explain why both PL peak position and FWHM become independent of x for such low In compositions.

For samples grown at 805°C $\leq T_g \leq$ 825°C ($0.105 \geq x \geq 0.054$) the PL FWHM is observed to broaden rapidly, with this broadening accompanied by a rapid decrease in PL efficiency. This is attributed to the effects of the onset of initial small strain relaxation (as opposed to the spinodal decomposition of the material into two subsystems: fully relaxed and only slightly relaxed, observed for $T_g <$ 800°C) and increasing point defect concentration, as discussed above.

As seen from the PLE spectra in Fig. 4, the native centre-like PL band is excited via the host matrix, which is consistent with that observed for doped centres in InAlN [25] and native defects found in other III-N alloys [26]. This allows the PL bands observed here to be used as a reliable probe of semiconductor band-gap. The InAlN effective band-gaps $E_{g,\,eff}$ derived from the PLE spectra using the sigmoidal expression [21], are plotted in Fig. 4 as a function of indium content. As can be seen from the spectra in Fig. 2 *b*, the samples grown at $T_g >$ 900°C clearly exhibit a double edge absorption, leading to their characterisation using double sigmoidal expression and thus with two $E_{g,\,eff}$ values. In most cases the error bar in determination of band gap is less than 10 meV; the only exception from this is the double sigmoidal fit of the $x = 0.008$ sample ($\delta E_g = \pm 30$ meV), for which the double absorption band is barely detectable.

We attribute the double edge PLE spectra observed for samples with $x \leq 0.008$ to the relative contributions to the PL of carriers photogenerated from different valence bands uniaxially split due to the wurtzite crystal field. The energy difference between the higher and lower band-edges (~0.22 eV) for these very low indium content samples matches typically published values for crystal field splitting in AlN [27], further corroborating our assertion. It should be noted that such a double-edge PLE behaviour has been reported previously by Feneberg et al. [26] in $Al_{1-y}Ga_yN$, and attributed to the same mechanism. However, in that case the effect exists for Ga contents up to at least $y = 0.06$, whereas here it is only observable for $In_xAl_{1-x}N$ where $x \leq 0.008$, i.e. approximately one order of magnitude smaller. This is consistent with recent theoretical analysis [8, 28] showing that In atoms cause a strong intermixing of the valence band states in the material. The finding is also consistent with the PLE double-absorption edge of InAlN samples disappearing rapidly with increasing In as the absorption of the material is dominated by the lower (fundamental) band-gap for 'high' x ($x > 0.02$) despite the nominally forbidden nature of the transition for *c*-plane material. Consequently, if the wave function character of the highest valence state switches at much higher AlN contents than one would predict from a linear interpolation of the valence band parameters, access to a significantly larger range of TE emitting structures might be expected. This finding is important for designing InAlN-based devices operating in the UV spectral region, since the light polarization characteristics affect the light extraction efficiency of the device. Similarly, for polar AlN-based photodetectors [29] it is clear that small amounts (<1%) of In will significantly modify the effective absorption edge due to a combination of this effect and the high bowing giving a high degree of sensitivity for photon energies around 6 eV.

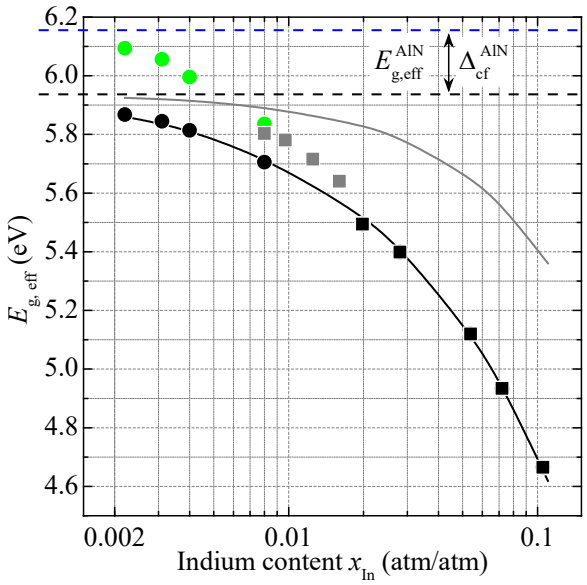

Fig. 4. Composition dependent effective band-gaps derived from PLE spectra by fitting with single (squares) or double sigmoidal expressions (circles). Black solid line – fit using band-anticrossing (BAC) model (see text below). Grey solid line – fit using linear interpolation between AlN and InN band-gaps.

As mentioned previously, RT PL was not observed from AlN samples under low intensity lamp excitation, leaving no opportunity to measure its PLE spectrum. We therefore required an alternative approach to determine a value of the AlN $E_{g,\,eff}$ compatible with our InAlN $E_{g,\,eff}$ plotted in Fig. 4. This was performed by extracting the AlN $E_{g,\,eff}$ value from PLE spectra of two identical InAlN layers, one of which was overgrown with 150 nm of AlN. This additional thin AlN layer acted as an optical filter for the InAlN, with its PLE spectrum modified accordingly for photon energies above the AlN band-gap, while below AlN band-gap the top layer becomes transparent leaving the PLE signal unaffected (Fig. 5). If one ignores any difference in the amount of reflected light, which is marginal in comparison to the absorption of light in the AlN cap, these two spectra are related by the simple expression:

$$I_{\mathrm{PLE,\,capped}}(h\nu) = I_{\mathrm{PLE,\,uncapped}}(h\nu) \cdot e^{-\alpha_{\mathrm{AlN}}(h\nu)\cdot d_{\mathrm{AlN}}}, \quad (4)$$

where $\alpha_{\mathrm{AlN}}(h\nu)$ is the AlN absorption spectrum and d_{AlN} is the thickness of the AlN layer grown on top of InAlN. From equation (4) we estimated the AlN absorption spectrum as:

$$\alpha_{\mathrm{AlN}}(h\nu) = \ln\left(I_{\mathrm{PLE,\,uncapped}}(h\nu)/I_{\mathrm{PLE,\,capped}}(h\nu)\right)/d_{AlN}. \quad (5)$$

This is plotted in Fig. 5, along with the above mentioned PLE spectra. Next the effective band-gap $E_{\mathrm{g,\,eff}}^{\mathrm{AlN}}$ was derived from the absorption spectrum using the same methodology as for the InAlN PLE spectra. Although this is rather an exotic method to estimate the homogeneous binary compound band-gap, giving a value most probably underestimated by at least the exciton binding energy [26], this value is most appropriate to be compared to our InAlN $E_{\mathrm{g,\,eff}}$ values given the similarity in method used to determine it. The $E_{\mathrm{g,\,eff}}^{\mathrm{AlN}}$ value obtained is 6.155 eV, which matches well to the classical ~6.2 eV RT AlN band-gap corresponding to the $\Gamma_{7c}\rightarrow\Gamma_{9v}$ transition after deduction of the exciton binding energy (~0.051 eV [30]). The fundamental effective band-gap $E_{\mathrm{g,\,eff}}^{\mathrm{AlN}}$ corresponding to the $\Gamma_{7c}\rightarrow\Gamma_{7vbm}$ transition (where "vbm" indicates valence band maximum) was not seen in the absorption spectrum, so it was taken as the difference of the $\Gamma_{7c}\rightarrow\Gamma_{9v}$ transition energy and the AlN crystal field splitting Δ_{cf}. Both values are shown by horizontal dashed lines in Fig. 4.

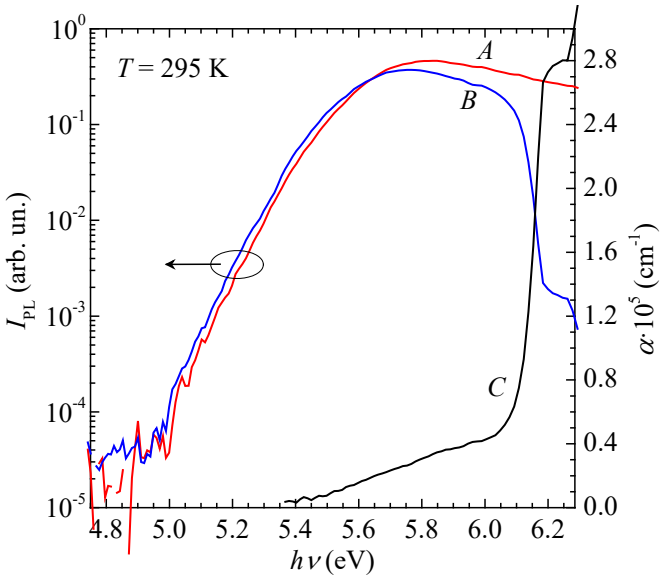

Fig. 5. PLE spectra of uncapped (curve *A*) and AlN-capped (curve *B*) $In_{0.019}Al_{0.981}N$ layers as well as the resulting absorption spectrum of AlN (curve *C*) determined from equation (5).

The rapid reduction in energy gap observed here with increasing In composition (Fig. 4) is consistent with the theoretical results in [8], where a strong band gap bowing was also observed for

small x_{In}. The first-principles calculations undertaken in [28] showed that In-related localized states are formed in the conduction and the valence band in $In_xAl_{1-x}N$ for low In composition, x, and that these resonant localized states dominate the evolution of the band structure with increasing x. The variation of the conduction band edge (CBE) energy with x in III-V alloys where one of the alloy components introduces resonant defect states above the CBE can be well described in low x range (dilute limit) by the BAC model [31-33]. In the BAC model, the evolution of the CBE energy is given by the lower eigenvalue of the 2 × 2 Hamiltonian matrix [31, 32, 34]:

$$H(x) = \begin{pmatrix} E_{\mathrm{D}}(x) & V_{\mathrm{D,\,c}} \\ V_{\mathrm{D,\,c}} & E_{\mathrm{c}}(x) \end{pmatrix}, \tag{6}$$

where $E_{\mathrm{D}}(x) = E_{\mathrm{In}}^{0} - \gamma \cdot x$ is the assumed variation of the mean In-related resonant defect energy with composition, and $E_{\mathrm{c}}(x) = E_{\mathrm{c,\,0}} - \alpha \cdot x$ describes the virtual crystal approximation (VCA) variation of the host matrix CBE state with In composition x. Here $E_{\mathrm{c,\,0}}$ is the CBE for AlN, which was taken as the difference between $E_{\mathrm{g,\,eff}}$ for AlN estimated above and AlN crystal field splitting (6.155 eV – 0.219 eV = 5.936 eV) to take into consideration the $\Gamma_{7c} \rightarrow \Gamma_{7vbm}$ transition. $V_{\mathrm{D,\,c}}$ describes the interaction between the levels, which varies with x as $\beta\sqrt{x}$, where the $\sqrt{x}$ dependence arises because the interaction is between a localized defect and extended conduction states [34]. The change of the CBE energy with In composition x is then given by the lower eigenvalue E_{-} of the Hamiltonian in Eq. (6)

$$E_{-}(x) = \frac{E_{\mathrm{c}} + E_{\mathrm{D}}}{2} - \sqrt{\left(\frac{E_{\mathrm{c}} - E_{\mathrm{D}}}{2}\right)^{2} + V_{\mathrm{D,\,c}}^{2}}. \tag{7}$$

As T_{g} decreases from 940°C, the relative contribution of the lower energy edge to PL is observed to increase (Fig. 2, *b*). The lower energy edge values determined from the double sigmoidal fit of PLE spectra for samples with $x \leq 0.008$ (Fig. 4, black circles) form a smooth x-dependence of the band-gap together with those obtained using the single sigmoidal fit for samples with $x \geq 0.02$ (Fig. 4, black squares) for which, taking into account the above mentioned tendency (Fig. 2, *b*), the

lower band-edge transition is expected to be dominant. We chose to fit these experimentally measured data for the variation in energy gap using Eq. (7). It can be seen that the BAC model (black solid curve in Fig. 4) gives a very good fit over the full composition range considered. The fit shown is obtained by assuming that the isolated In-related defect level E_{In}^{0} is 0.3 eV above the AlN CBE, that $\alpha = \gamma = 3$ eV, and that $\beta = 3.4$ eV. We note that the values used here are slightly larger than those used to fit the theoretical conduction band data in [28]. In [28] a nonparabolicity was found in both the valence and the conduction band edges of InAlN. Here, we have basically constructed an "effective" BAC model. Effects arising from the evolution of both the conduction and the valence band with composition *x* are condensed into one set of BAC parameters. Hence, it is not unexpected that the parameters extracted here are larger than the values we got for the conduction band alone in [28]. In addition, with four free parameters in Eq. (4), it is clear that a range of other values could have been chosen to fit to the experimental data. Nevertheless, the overall analysis strongly supports our previous theoretical work [28] stating that localized In states, both in the valence and the conduction band, significantly affect the composition dependence of the InAlN band-gap, E_{g} and give rise to the nonparabolicity of E_{g} reported here.

The grey solid line in Fig. 4 shows the expected variation of energy gap with composition in $In_xAl_{1-x}N$ assuming a linear interpolation between the energy gaps of AlN and InN (i.e. ignoring any band-gap bowing). As discussed earlier, such a linear variation significantly overestimates the energy gap; while the excellent fit with the solid black line confirms that the evolution of the band-gap in $In_xAl_{1-x}N$ can be very well described for low values of *x* using a BAC model to take account of the interaction between localized In states and the host matrix band edges. It should be noted that the rapid change of band-gap with *x* for the samples reported here cannot be combined with previous results for higher values of *x* to obtain a "classical" composition independent parabolic bowing parameter, consistent with previously reported analyses [7, 13].

Since the data in Fig. 4 represent the composition dependence of the effective band-gap $E_{\mathrm{g,\,eff}}(x)$, it is worth converting the data to provide an x-dependent band-gap bowing parameter $b(x)$, using the following expression:

$$b(x) = \frac{(1-x)\cdot E_{\mathrm{g,\,eff}}^{\mathrm{AlN}} + x \cdot E_{\mathrm{g,\,eff}}^{\mathrm{InN}} - E_{\mathrm{g,\,eff}}^{\mathrm{InAlN}}(x)}{x\cdot(1-x)}. \tag{8}$$

As seen from the above formula, the term $b(x)$ becomes extremely sensitive to the $E_{\mathrm{g,\,eff}}^{\mathrm{AlN}}$ value chosen at small indium contents. Even though AlN has been studied for a long time, there is still some discrepancy in the RT band-gap values (6.01-6.22 eV) reported in the literature [35 and references therein]. Partly this is caused by the fact that only the higher energy transition $\Gamma_{7c}\rightarrow\Gamma_{9v}$ can be effectively "seen" for commonly used *c*-plane AlN epitaxial samples, which is then sometimes considered to be the fundamental transition, instead of $\Gamma_{7c}\rightarrow\Gamma_{7vbm}$, as discussed by Li et al. [27]. There is another more important impediment when using data from the literature for $E_{\mathrm{g,\,eff}}^{\mathrm{AlN}}$: Because InAlN has a fairly "soft" absorption edge, similar to InGaN [21], it can be characterised only by an effective band-gap value, while values for AlN in the literature are claimed to be defined conventionally. We therefore need (and indeed already have from the AlN band-gap analysis obtained from the PLE spectra presented in Fig. 5 and discussed earlier) a value which is compatible with our $E_{\mathrm{g,\,eff}}^{\mathrm{InAlN}}(x)$ data. At the same time, as seen from equation (8), $b(x)$ is much less dependent on $E_{\mathrm{g,\,eff}}^{\mathrm{InN}}$ for low indium containing InAlN; hence, it is sufficient to use literature data for $E_{\mathrm{g,\,eff}}^{\mathrm{InN}}$, despite there also being a fairly large scatter in experimental values for $E_{\mathrm{g,\,eff}}^{\mathrm{InN}}$ (varying between 0.62 and 0.8 eV [36, 37]). As a compromise we used a value of 0.65 eV for $E_{\mathrm{g,\,eff}}^{\mathrm{InN}}$. Experimental values of b were then determined using equation (8) and are plotted as a function of x in Fig. 6 (squares).

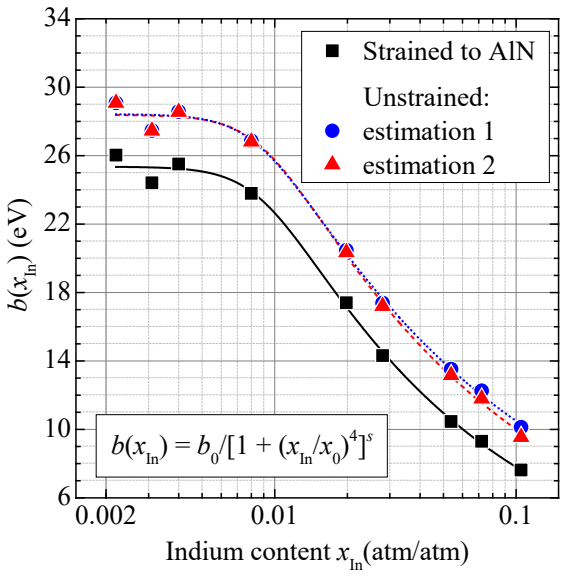

Fig. 6. Composition dependent band-gap bowing parameter for InAlN strained to AlN (squares) and corrected for the unstrained case (circles and triangles). The lines plotted using the specified empirical expression with parameters listed in the Table are guides to the eye.

It should be noted that the experimental data presented in Fig. 4 relate to the bandgap of InAlN compressively strained to AlN; therefore, the band gap is expected to be overestimated in comparison to that of unstrained InAlN. To correct the data for the unstrained material one needs to take into account the strain dependence of the InAlN band-gap. Unfortunately, data regarding this strain dependence are not directly available in the literature; however, an estimate can still be made based on the relevant data currently available for AlN, InN and $In_xAl_{1-x}N$.

The variation with strain of the AlN direct energy gap $E_{g,\,A}$ (due to transition $\Gamma_{7c} \rightarrow \Gamma_{7vbm}$) and of the $E_{g,\,B/C}$ energy gap ($\Gamma_{7c} \rightarrow \Gamma_{9v}/\Gamma_{7v}$ transitions) are given respectively by [38]

$$E_{g,\,A} = E_{g,\,A,\,0} + \left(a_{cz}^{AlN} - D_1^{AlN}\right) \cdot \varepsilon_{zz} + \left(a_{ct}^{AlN} - D_2^{AlN}\right) \cdot \left(\varepsilon_{xx} + \varepsilon_{yy}\right) \qquad (9)$$

and

$$E_{g,\,B/C} = E_{g,\,B/C,\,0} + \left(a_{cz}^{AlN} - D_1^{AlN} - D_3^{AlN}\right) \cdot \varepsilon_{zz} + \left(a_{ct}^{AlN} - D_2^{AlN} - D_4^{AlN}\right) \cdot \left(\varepsilon_{xx} + \varepsilon_{yy}\right), \qquad (10)$$

where $E_{\mathrm{g,\,A/B/C,\,0}}$ are energy gaps of unstrained material, ε_{xx} and ε_{yy} are the in-plane strain components, ε_{zz} is the strain along the *c*-axis direction, and $a_{\mathrm{cz}}^{\mathrm{AlN}}$, $a_{\mathrm{ct}}^{\mathrm{AlN}}$ and D_i^{AlN} are AlN deformation potentials, with D_3^{AlN} and D_4^{AlN} the deformation potentials describing the strain dependence of the crystal field splitting. For biaxially strained layers, such as those considered here, $\varepsilon_{yy} = \varepsilon_{xx}$ and $\varepsilon_{zz} = -R_c\varepsilon_{xx}$, where the biaxial relaxation coefficient $R_c = 2C_{13}/C_{33}$, with C_{13} and C_{33} elastic constants. For $In_xAl_{1-x}N$ at low In composition ($x <\sim 10\%$), R_c has a very weak dependence on *x* [39], so we use the AlN value $R_c = 0.62$ from [39] in our analysis below, independent of In composition.

Taking into account the above relations between strain components, expressions (9) and (10) can be simplified to the form: $\Delta E_{\mathrm{g}}(\varepsilon_{xx}) = E_{\mathrm{g}}(\varepsilon_{xx}) - E_{\mathrm{g,\,0}} = k \cdot \varepsilon_{xx}$ with $k_{\mathrm{A}} = 2 \cdot (a_{\mathrm{ct}} - D_2) - R_c \cdot (a_{\mathrm{cz}} - D_1)$ and $k_{\mathrm{B}} = 2 \cdot (a_{\mathrm{ct}} - D_2 - D_4) - R_c \cdot (a_{\mathrm{cz}} - D_1 - D_3)$ for $\Gamma_{7c}\rightarrow\Gamma_{7vbm}$ and $\Gamma_{7c}\rightarrow\Gamma_{7v}/\Gamma_{9v}$ transitions respectively. Assuming for now that k varies linearly with In composition *x*, ($k_{\mathrm{InAlN}} = k_{\mathrm{InN}} + (k_{\mathrm{AlN}} - k_{\mathrm{InN}}) \cdot x$) and using as endpoints k_{A} values of k_{InN} = –6.9 eV and k_{AlN} = –22 eV, based on the deformation potentials from [38], a bandgap correction can be made for each sample. For instance, taking into account the strain value of –1.15% for our ~20% relaxed $In_{0.105}Al_{0.895}N$ sample, and using k_{A} = 20.4 eV gave a reduction in energy gap of 0.235 eV for unstrained $In_{0.105}Al_{0.895}N$ compared to the value measured here (estimation 1, “linear”).

However two factors are likely to lead to a smaller actual difference in energy gap between the strained and unstrained alloys. Firstly, it has been shown both theoretically and experimentally that the hydrostatic pressure dependence of the energy gap, dE_{g}/dp is dramatically reduced for $In_xAl_{1-x}N$ with low In composition compared to that of AlN [40]. Depending on the type of alloy assumed, the calculated band-gap pressure coefficient reaches that of InN already at 40% and 15% In, in the case of homogeneously ordered and clustered alloys respectively. This indicates a strongly nonlinear composition dependence of the deformation potentials a_{ci} and D_i in $In_xAl_{1-x}N$. Therefore our assessment using a linear composition dependence of k most likely overestimates the energy gap

reduction. There is insufficient information in the literature to deduce the nonlinear composition dependence of the deformation potentials in Eq. (9). However, it can be expected that much of the reduction in deformation potentials should occur at very low In compositions, consistent with what is observed using the BAC model in other alloys such as $GaInN_xAs_{1-x}$ [41]. If we assume that most of the reduction in deformation potentials occurs by 25% indium (consistent with the data on dE_g/dp in [40]) this would then give a reduction in energy gap of 0.18 eV for the $In_{0.105}Al_{0.895}N$ layer here (estimation 2, "bowing").

Correcting our band-gap data for the strain using these two assumptions led to the revised bowing parameters plotted in Fig. 6 as circles ("linear") and triangles ("bowing"). The experimental data in Fig. 6 were fitted with empirical equation given in the figure. The best fit was achieved using parameters listed in the Table below for each case.

Secondly, even the assessment taking into account bowing of InAlN deformation potentials may still overestimate the change in energy gap. From the PLE data, it can be seen that Γ_{9v} character starts to mix into the highest valence states in $In_xAl_{1-x}N$ for very low In content x. If we assume that the Γ_{9v} character dominates the strain dependence of the band edge states, then we should use Eq. (10) to estimate the change in band gap. Using a linear interpolation gives $k_B = -8.14$ eV and an energy gap change of only 94 meV for the x = 10.5% sample.

Table. – Parameters of empirical expression specified in Fig. 6 allowing for the best fit of the data presented there.

Parameter / **Case**	b_0 (eV)	x_0 (atm/atm)	s
Strained to AlN (experimental)	25.4±0.3	0.0090±0.0009	0.122±0.007
Unstrained (estimation 1, "linear")	28.4±0.3	0.0087±0.0008	0.102±0.006
Unstrained (estimation 2, "bowing")	28.4±0.3	0.0091±0.0008	0.109±0.006

The InAlN band-gap can be now calculated applying the conventionally used equation:

$$E_{\mathrm{g}}^{\mathrm{InAlN}}(x) = E_{\mathrm{g}}^{\mathrm{AlN}} - x \cdot \left(E_{\mathrm{g}}^{\mathrm{AlN}} - E_{\mathrm{g}}^{\mathrm{InN}}\right) - b(x) \cdot x \cdot (1 - x). \quad (9)$$

It should be noted in the above that it is critical to use the lower $\Gamma_{7c} \rightarrow \Gamma_{7vbm}$ measure of the band-gap for AlN irrespective of the crystallographic orientation of the sample under consideration. Using the empirical expression for bowing parameter in Fig. 6 and Eq. (9), one can accurately estimate the band-gap of low In containing InAlN alloys.

4. Conclusions

In summary, we reported on the optical properties of 80-120 nm thick $In_xAl_{1-x}N$ epitaxial layers prepared on AlN templates with low In content. The layers are found to be nearly fully strained for In compositions less than about 0.10. While no luminescence was observed for relaxed samples ($x > 0.11$) those that were fully strained exhibited strong near UV luminescence with maximum efficiency for indium content in the range 0.004-0.016. The luminescence centre(s) responsible for the band are currently not identified, though a clear association with the presence of In is observed. Using the band as a probe for photoluminescence excitation spectroscopy a detailed determination of the variation of the room temperature $In_xAl_{1-x}N$ effective band-gap with indium content in the range $0.0022 < x < 0.11$ was obtained. The band-gap was found to decrease rapidly with indium content resulting in $In_xAl_{1-x}N$ band-gap bowing parameter of above 25 eV in the $x \rightarrow 0$ limit. The obtained evolution of the $In_xAl_{1-x}N$ band-gap in the $x < 0.11$ range can be very well described using a band-anticrossing model to take account of the interaction between localized In states and the host matrix conduction and valence band edges. This data allows determination of the potential of InAlN for active region design and reflector stacks in the UV, as well as for modelling of InAlN based heterostructure field effect transistors. Furthermore, the presented data shows the strong impact of a small (<1%) content of InN in an AlN matrix on the selection rules governing surface emission and absorption in InAlN, of direct relevance in the consideration of such alloys for UV emitter applications.

Acknowledgments

This research was enabled by Science Foundation Ireland (SFI) under grant Nos. SFI/10/IN.1/I2993, 10/IN.1/I2994 and 13/SIRG/2210, the Irish Higher Education Authority Programme for Research in Third Level Institutions Cycles 4 and 5 via the INSPIRE and TYFFANI projects and the European Union 7th Framework Programme DEEPEN (grant agreement no. 604416). D. V. D. acknowledges funding support from the European Union 7th Framework Programme ALIGHT project (agreement no. FP7-280587). S. N. A. acknowledges studentship funding from Iranian Ministry of Science, Research and Technology. P. J. P. acknowledges funding from SFI Engineering Professorship scheme (SFI/07/EN/E001A).

References

[1] J.-F. Carlin and M. Ilegems, High-quality AlInN for high index contrast Bragg mirrors lattice matched to GaN, Appl. Phys. Lett. **83**, 668 (2003).

[2] A. Dadgar, F. Schulze, J. Bläsing, A. Diez, A. Krost, M. Neuburger, E. Kohn, I. Daumiller, and M. Kunze, High-sheet-charge–carrier-density AlInN⁄GaN field-effect transistors on Si(111), Appl. Phys. Lett. **85**, 5400 (2004).

[3] S. Senda, H. Jiang and T. Egawa, AlInN-based ultraviolet photodiode grown by metal organic chemical vapor deposition, Appl. Phys. Lett. **92**, 203507 (2008).

[4] S. Nicolay, J.-F. Carlin, E. Feltin, R. Butté, M. Mosca, N. Grandjean, M. Ilegems, M. Tchernycheva, L. Nevou, and F. H. Julien, Midinfrared intersubband absorption in lattice-matched AlInN/GaN multiple quantum wells, Appl. Phys. Lett. **87**, 111106 (2005).

[5] V. Z. Zubialevich, T. C. Sadler, D. V. Dinh, S. N. Alam, H. N. Li, P. Pampili, and P. J. Parbrook, Enhanced UV luminescence from InAlN quantum well structures using two temperature growth, J. of Luminesc. **155**, 108 (2014).

[6] L. Zhang, K. Dong, D. Chen, Y. Liu, J. Xue, H. Lu, R. Zhang and Y. Zheng, Solar-blind ultraviolet AlInN/AlGaN distributed Bragg reflectors, Appl. Phys. Lett. 102, 242112 (2013).

[7] E. Iliopoulos, A. Adikimenakis, C. Giesen, M. Heuken, and A. Georgakilas, Energy bandgap bowing of InAlN alloys studied by spectroscopic ellipsometry, Appl. Phys. Lett. **92**, 191907 (2008).

[8] S. Schulz, M. A. Caro, L.-T. Tan, P. J. Parbrook, R. W. Martin, and E. P. O'Reilly, Composition-Dependent Band Gap and Band-Edge Bowing in AlInN: A Combined Theoretical and Experimental Study, Appl. Phys. Express **6**, 121001 (2013)

[9] T. Matsuoka, Calculation of unstable mixing region in wurtzite $In_{1-x-y}Ga_xAl_yN$, Appl. Phys. Lett. **71**, 105 (1997).

[10] J. Kim, Z. Lochner, M.-H. Ji, S. Choi, H. J. Kim, J. S. Kim, R. D. Dupuis, A. M. Fischer, R. Juday, Y. Huang, T. Li, J. Y. Huang, F. A. Ponce, J.-H. Ryou, Origins of unintentional incorporation of gallium in InAlN layers during epitaxial growth, part II: Effects of underlying layers and growth chamber conditions, J. Cryst. Growth **388**, 143 (2014).

[11] M. D. Smith, E. Taylor, T. C. Sadler, V. Z. Zubialevich, K. Lorenz, H. N. Li, J. O'Connell, E. Alves, J. D. Holmes, R. W. Martin and P. J. Parbrook, Determination of Ga auto-incorporation in nominal InAlN epilayers grown by MOCVD, J. Mater. Chem. C **2**, 5787 (2014).

[12] L. Nordheim, Zur Elektronentheorie der Metalle. I, Ann. Phys. (Leipzig) **9**, 607 (1931) [in German].

[13] E. Sakalauskas, H. Behmenburg, C. Hums, P. Schley, G. Rossbach, C. Giesen, M. Heuken, H. Kalisch, R. H. Jansen, J. Bläsing, A. Dadgar, A. Krost, and R. Goldhahn, Dielectric function and optical properties of Al-rich AlInN alloys pseudomorphically grown on GaN, J. Phys. D **43**, 365102 (2010).

[14] M. Ferhat and F. Bechstedt, First-principles calculations of gap bowing in $In_xGa_{1-x}N$ and $In_xAl_{1-x}N$ alloys: Relation to structural and thermodynamic properties, Phys. Rev. B **65**, 075213 (2002).

[15] Z. Dridi, B. Bouhafs and P. Ruterana, First-principles investigation of lattice constants and bowing parameters in wurtzite $Al_xGa_{1-x}N$, $In_xGa_{1-x}N$ and $In_xAl_{1-x}N$ alloys, Semicond. Sci. Technol. **18**, 850 (2003).

[16] H.-Y. Ryu, Large enhancement of light extraction efficiency in AlGaN-based nanorod ultraviolet light-emitting diode structures, Nanosc. Research Lett. **9**, 58 (2014).

[17] K. S. Kim, A. Saxler, P. Kung, M. Razeghi, and K. Y. Lim, Determination of the band-gap energy of $Al_{1-x}In_xN$ grown by metal–organic chemical-vapor deposition, Appl. Phys. Lett. **71**, 800 (1997).

[18] R. R. Pelá, C. Caetano, M. Marques, L. G. Ferreira, J. Furthmüller, and L. K. Teles, Accurate band gaps of AlGaN, InGaN, and AlInN alloys calculations based on LDA-1/2 approach, Appl. Phys. Lett. **98**, 151907 (2011)

[19] H. N. Li., T. C. Sadler and P. J. Parbrook, AlN heteroepitaxy on sapphire by metalorganic vapour phase epitaxy using low temperature nucleation layers, J. Cryst. Growth **383**, 72 (2013).

[20] N. Nepal, J. Li, M. L. Nakarmi, J. Y. Lin, and H. X. Jiang, Temperature and compositional dependence of the energy band gap of AlGaN alloys, Appl. Phys. Lett. **87**, 242104 (2005).

[21] R. W. Martin, P. G. Middleton, K. P. O`Donnell and W. Van der Stricht, Exciton localization and the Stokes' shift in InGaN epilayers, Appl. Phys. Lett. **74**, 263 (1998).

[22] Z. Y. Fan, G. Rong, and N. Newmana, D. J. Smith, Defect annihilation in AlN thin films by ultrahigh temperature processing, Appl. Phys. Lett. **76**, 1839 (2000).

[23] S. F. Chichibu, A. Uedono, T. Onuma, S. P. DenBaars, U. K. Mishra, J. S. Speck, S. Nakamura, Impact of Point Defects on the Luminescence Properties of (Al,Ga)N, Mater. Sci. Forum **590**, 233-248 (2008).

[24] S. F. Chichibu, K. Hazu, K. Furusawa, Y. Ishikawa, T. Onuma, T. Ohtomo, H. Ikeda, and K. Fujito, High internal quantum efficiency ultraviolet to green luminescence peaks from pseudomorphic *m*-plane $Al_{1-x}In_xN$ epilayers grown on a low defect density *m*-plane freestanding GaN substrate, J. Appl. Phys. **116**, 213501 (2014).

[25] I. S. Roqan, K. P. O'Donnell, R. W. Martin, C. Trager-Cowan, V. Matias, A. Vantomme, K. Lorenz, E. Alves, and I. M. Watson, Optical and structural properties of Eu-implanted $In_xAl_{1-x}N$, J. Appl. Phys. **106**, 083508 (2009)

[26] M. Feneberg, M. Röppischer, N. Esser, C. Cobet, B. Neuschl, T. Meisch, K. Thonke, and R.Goldhahn, Synchrotron-based photoluminescence excitation spectroscopy applied to investigate the valence band splittings in AlN and $Al_{0.94}Ga_{0.06}N$, Appl. Phys. Lett. **99**, 021903 (2011).

[27] J. Li, K. B. Nam, M. L. Nakarmi, J. Y. Lin, H. X. Jiang, P. Carrier, and S.-H. Wei, Band structure and fundamental optical transitions in wurtzite AlN, Appl. Phys. Lett. **83**, 5163 (2003).

[28] S. Schulz, M. A. Caro, and E. P. O'Reilly, Impact of cation-based localized electronic states on the conduction and valence band structure of $Al_{1-x}In_xN$ alloys, Appl. Phys. Lett. **104**, 172102 (2014).

[29] J. Li, Z. Y. Fan, R. Dahal, M. L Nakarmi, J. Y. Lin and H. X. Jiang, 200 nm deep ultraviolet photodetectors based on AlN, Appl. Phys. Lett. **89**, 213510 (2006).

[30] S. F. Chichibu, K. Hazu, Y. Ishikawa, M. Tashiro, T. Ohtomo, K. Furusawa, A. Uedono, S. Mita, J. Xie, R. Collazo, and Z. Sitar, Excitonic emission dynamics in homoepitaxial AlN films studied using polarized and spatio-time-resolved cathodoluminescence measurements, Appl. Phys. Lett. **103**, 142103 (2013).

[31] W. Shan, W. Walukiewicz, J. W. Ager, E. E. Haller, J. F. Geisz, D. J. Friedman, J. M. Olson, and S. R. Kurtz, Band Anticrossing in GaInNAs Alloys, Phys. Rev. Lett. **82**, 1221 (1999).

[32] A. Lindsay and E. P. O'Reilly, Unification of the Band Anticrossing and Cluster-State Models of Dilute Nitride Semiconductor Alloys, Phys. Rev. Lett. **93**, 196402 (2004).

[33] E. P. O'Reilly, A. Lindsay, P. J. Klar, A. Polimeni and M. Capizzi, Trends in the electronic structure of dilute nitride alloys, Semicond. Sci. Technol. **24**, 033001 (2009).

[34] E. P. O'Reilly, A. Lindsay, Theory of enhanced bandgap non-parabolicity in GaN_xAs_{1-x} and related alloys, Solid. State. Commun. **112**, 443 (1999).

[35] I. Vurgaftman and J. R. Meyer, Band parameters for nitrogen-containing semiconductors, J. Appl. Phys. **94**, 3675 (2003).

[36] S. P. Fu, T. T. Chen and Y. F. Chen, Photoluminescent properties of InN epifilms, Semicond. Sci. Technol. **21**, 244 (2006)–249.

[37] Y. Nanishi, Y. Saito and T. Yamaguchi, RF-Molecular Beam Epitaxy Growth and Properties of InN and Related Alloys, Jpn. J. Appl. Phys. **42**, 2549 (2003).

[38] Q. Yan, P. Rinke, A. Janotti, M. Scheffler, and C. G. Van de Walle, Effects of strain on the band structure of group-III nitrides, Phys. Rev. B 90, 125118 (2014)

[39] S. P. Lepkowski and I. Gorczyca, Poisson Ratio and Biaxial Relaxation Coefficient in $In_xGa_{1-x}N$ and $In_xAl_{1-x}N$ Alloys, Acta Physica Polonica A, 120, 902-904 (2011)

[40] I. Gorczyca, A. Kaminska, G. Staszczak, R. Czernecki, S. P. Lepkowski, T. Suski, H. P. D. Schenk, M. Glauser, R. Butte, J. F. Carlin, E. Feltin, N. Grandjean, N. E. Christensen, and A. Svane, Anomalous composition dependence of the band gap pressure coefficients in In-containing nitride semiconductors, Phys. Rev. B 81, 235206 (2010)

[41] W. Shan, W. Walukiewicz, J. W. Ager III, E. E. Haller, J. F. Geisz, D. J. Friedman, J. M. Olson and S. R. Kurtz, Band Anticrossing in GaInNAs Alloys, Phys. Rev. Lett. 82, 1221 (1999).